Dalton Transactions

Accepted Manuscript

ROYAL SOCIETY OF CHEMISTRY

www.rsc.org/dalton

Dalton Transactions

COMMUNICATION

Rounded Cu_2ZnSnS_4 Nanosheet Networks as Cost-effective Counter Electrode for High-Efficiency Dye-Sensitized Solar Cells

Received 00th January 20xx,
Accepted 00th January 20xx

DOI: 10.1039/x0xx00000x

www.rsc.org/

Shan-Long Chen,[ab] Jie Tao,[a*] Hai-Jun Tao,[ab] Yi-Zhou Shen,[a] Ai-Chun Xu,[a] Fang-Xu Cao,[a] Jia-Jia Jiang,[a] Tao Wang[a] and Lei Pan[a]

Semi-transparent rounded Cu_2ZnSnS_4 (CZTS) nanosheet networks were in-situ grown on FTO glass substrate, via a effective solution method, without any post-treatments. An improved power conversion efficiency of 6.24 % was obtained by applying CZTS nanosheet networks as counter electrode for dye-sensitized solar cells. When assisted by a mirror reflection, the PCE increased to 7.12 %.

The rapid expansion of cost-effective counter electrode (CE) catalysts for dye-sensitized solar cells (DSSCs) has drawn extensive research interest.[1-7] As an important component in DSSCs, the CE materials should possess two advantages of high catalytic activity and electrical conductivity.[8,9] The high cost and low natural abundance, and poor corrosion resistance of Pt hinder the commercialization of DSSCs.[10] Hence, to address the problem of high cost and instability for Pt CE, many alternative Pt-free materials have been proposed to be used as CE catalysts, including carbon materials,[11-13] conducting polymers,[14] and the inorganic compounds (transition metal in the form of oxides, nitrides, carbides, and sulfides).[8] In particular, SnS(Se),[15] CuSe(S),[16] $FeSe_2$,[16,17] $Ni_{0.85}(Co_{0.85})Se$,[18] Co_9S_8,[19] $NiSe_2$,[20] NiS,[21,22] NiS_2,[23-25] Sb_2S_3,[26] $MoSe(S)_2$,[27,28] $CuInS_2$,[29] Cu_2FeSnS_4,[30] etc. have been investigated as Pt-free CE materials in recent years and they have shown excellent catalytic activity towards I^-/I_3^- electrolyte. Among them, notably, p-type kesterite-structure Cu_2ZnSnS_4 (CZTS) has been verified to be a high catalytic CE material, due to its advantages of earth abundance, low-toxicity, a direct band gap of 1.5 eV, and excellent catalytic ability towards I_3^- electrolyte. The performance of the DSSCs with CZTS is comparable to that of the cell with Pt, indicating the CZTS is alterative material to Pt in DSSCs.[31,32] Many techniques have been proposed to fabricate CZTS thin film CE, such as vacuum based deposition,[33,34] chemical vapour deposition, electrodeposition,[35] and solution-based processing.[36-43] The related CZTS-based device properties of the above reports are summarized in Table S1. Among the fabrication methods proposed above, the solution-based processing techniques have shown their remarkable potential for constructing low-cost, large-scale, and high-performance DSSCs. Furthermore, it is easy to acquire hierarchical nanostructure film with a large surface area, via varying the solvent, reactant, and long-chain surfactant, as the catalytic activity of a CE can be improved by altering the nanostructure of the material surface. Nevertheless, in a typical solution-based fabrication route, the nanostructure CZTS precursor film was firstly formed via spin, spray, or drop coating the CZTS inks/precursor solution on the substrate. Then, rigorous synthesis techniques are needed to meet the goals of pure phase, high crystallization and super catalytic activity, such as high temperature annealing or sulfurization (300 ^{o}C-600 ^{o}C in vacuum or sulfur-based vapour).[44] Hence, it is necessary to in-situ grow good-crystallinity, good-stability, and high-performance nanostructure CZTS thin film on substrate, through a feasible, cost-effective, green, and mild solution-based method, without any post-treatments.

In this communication, we present an effective solution method to synthesize CZTS nanostructure networks in situ on FTO glass substrate and utilize it directly as CE to assemble DSSCs without any post-treatments, such as annealing, sulfurization, or coating with other ancillary materials. The fabrication process is schematically indicated in Figure S1 and full experimental details are provided in the ESI. Briefly, the Cu-Zn-Sn alloy composites were firstly electrodeposited on a FTO substrate and then were transferred to CZTS phase directly by solvothermal treatment. During the solvothermal treatment, sodium thiosulfate ($Na_2S_2O_3$) powders serve as the sulfur source, but not sulfur powders. The $S_2O_3^{2-}$ transforms to H_2S and SO_4^{2-} anions through a disproportionation process.[45,46] The obtained SO_4^{2-} and adsorbed trace water molecules function as a protective layer on the surface of the as-

[a] College of Material Science and Technology, Nanjing University of Aeronautics and Astronautics, Nanjing 210016, P R China. E-mail: taojie@nuaa.edu.cn; Tel: (+86) 025-5211 2911.
[b] Jiangsu Province Key Laboratory of Materials and Technology for Energy Conversion, Nanjing University of Aeronautics and Astronautics, Nanjing 210016, P R China. E-mail: Shanlongchen@nuaa.edu.cn; Tel: (+86) 025-5211 2911.
† Footnotes relating to the title and/or authors should appear here.
Electronic Supplementary Information (ESI) available: [details of any supplementary information available should be included here]. See DOI: 10.1039/x0xx00000x

prepared CZT precursor and could promote the formation of uniform inter-connected CZTS nanosheet networks structure, as a result of shape control.[46] Then, the H_2S is also further decomposed to S^{2-} species. In addition, the surface of the porous CZT film has many small grain boundaries, then ethanol and the above sulfur species can easily permeate into the film to react with CZT compound to form sulfide at low temperature and high pressure. The whole process is described as follows:

$$S_2O_3^{2-}+H_2O \rightarrow SO_4^{2-}+H_2S \quad (1)$$

$$H_2S \rightarrow 2H^+ + S^{2-} \quad (2)$$

$$2Cu+Zn+Sn+4S^{2-} \rightarrow Cu_2ZnSnS_4\downarrow \quad (3)$$

Therefore, it is obvious that the existence of sodium thiosulfate in this work plays an important role in determining and controlling the morphology of CZTS. Optical and filed-emission scanning electron microscope (FE-SEM) images of the as-prepared CZTS film are clearly presented in Figure 1. It is apparent that CZT film is just as smooth and bright as a reflective mirror, and the solvothermal-obtained light-brown CZTS film is translucent from the optical images. The excellent transmittance suggests the CZTS film potential for more light coming into the cells from counter electrode, so as to boost the photovoltaic performance. From Figure 1 (a), the porous and rough precursor CZT film is composed of homogeneous aggregated particles, with the diameter of ca. 50-65 nm. Notably, after conversion process for 6 h, the resulting CZTS film shows a ca. ~540 nm thick homogeneous and compact layer, adhered to the substrate tightly. Moreover, the whole FTO substrate is uniformly covered by rounded CZTS nanosheet with width of ca. 380-580 nm and thickness of ca. 50-70 nm. The surface of CZTS sheet is extremely rough and composed of numerous nanoparticles with expanding specific surface area. This inter-connected nanosheet networks structure is beneficial to higher catalytic activity, as more electrolyte can anchor on the CZTS nanosheet and the photo-generated electrons can transfer through the sheet arrays into the conductive substrate fast and effectively.[47] Furthermore, all the elements are homogeneously spread over the whole area of substrate (Figure S2 (b-e)).

The phase-structural information of the as-synthesized CZTS CE is illustrated in Figure 2. The observed diffraction peaks show that kesterite-structure CZTS films (JCPDS 26-0575) are obtained during solvothermal treatment. The strong diffraction peaks around 28.5° and 47.3° are assigned to those crystal faces of (112) and (220) respectively. Furthermore, it is noteworthy that the XRD profiles of tetragonal Cu_2SnS_3 (JCPDS 89-4714) and cubic ZnS (JCPDS 80-0020) are similar to that of kesterite CZTS phase.[32,42] The further structural information of the sample is obtained from Raman spectrum. The peaks from Cu_2SnS_3 (352 cm^{-1}), ZnS (278, 346 cm^{-1}), and $Cu_{2-x}S$ (475 cm^{-1}) phases are not observed in Figure 2 (b). The Raman peak at 335 cm^{-1} and 288 cm^{-1} are from kesterite CZTS phase. These results exclude the presence of other binary or ternary sulfide compounds, with only CZTS existing.[35-40] To further study the detailed structures of the products, TEM measurement was subsequently performed. The two-dimensional characteristic of the nanosheet structures was confirmed. Moreover, the corresponding selected-area electron diffraction (SAED) pattern of the tetragonal-structure CZTS plate displays several diffraction dots, demonstrating that it is single crystals with great crystallinity. The presence of the major diffraction dots (112), (200), (220), and (312) is in good agreement with those reported in the literature. No apparent additional sulfide phases are observed and the pure phase of the CZTS film is further confirmed. From Figure 2 (d), HR-TEM image shows a set of crystallographic plane clearly, which corresponds to the (112) planes of kesterite-structure CZTS.

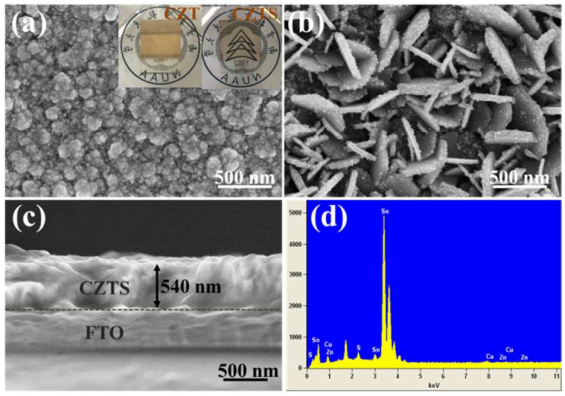

Figure 1. FE-SEM images of (a) CZT particle film and (b) rounded CZTS nanosheet on FTO substrate. The insert shows the digital photograph of CZT film and CZTS counter electrode. (c) Cross-sectional FE-SEM image of the CZTS film, reflecting a good bonding strength between in-situ CZTS film and FTO substrate. (d) The EDS spectra of CZTS film grown on FTO substrate.

Photocurrent density-voltage (J-V) curves of DSSCs, assembled with CZTS and Pt CEs, were obtained under a light intensity of 100 mW/cm^2. The photovoltaic parameters are listed in Table 1 and each value for cell performance is determined as an average of at least three devices. It is indicated that the DSSCs with rounded CZTS nanosheet CE possess an great cell performance (η=6.24%), which is superior to that of the DSSCs with Pt (η=6.01%). The CZTS CE has a higher fill factor (FF=62.92) than that of the Pt CE (FF=61.42), resulting in higher power conversion efficiency (PCE). The enhanced FF is attributable to the lower R_S and R_{Ct} from the EIS tests, demonstrating an improvement in charge transfer at the CE/electrolyte interface and low recombination rates (confirmed by dark current test in Figure S3).[17,48,49] Furthermore, a reflective mirror was used to improve the visible light utilization rate of the CZTS CE to achieve high transmittance, as shown in Figure 3 (a). The J_{SC} increases from 12.52 to 14.31 mA/cm^2, when reflecting the light penetrating through the solar cell, and the PCE increases from 6.24 to 7.12 % accordingly. The high catalytic ability of rounded CZTS nanosheet networks in DSSCs could be caused by the following reason: First, plate-based catalytic networks not only increase

catalytic surface area of electrode film but also accelerate the photo-generated electron transport at the counter electrode/redox electrolyte interface;[33,49] Second, according to the quantum chemistry predictions, the (202) surface of metal sulfide has overpotential behaviour in O_2 reduction similar to that observed for platinum electrodes, indicating the special surface structure of metal sulfide benefits the reduction of I_3^- ions.[50,51] Furthermore, it is also important to note that chemical stability toward the electrolyte and mechanical stability are the fundamental requirements for the stable and high-efficiency CZTS electrode. The long-term stability test of DSSCs based on CZTS CE was implemented for 7 days, as shown in Figure S4. After 7 days, the parameters of the FF, and efficiency retained 98, and 97 % of the initial values, respectively. A mechanical peel-off test was also performed, by sticking 3M Scotch tape on the surface of CZTS film and then peeling the tape off, to investigate the mechanical stability. After 10 times peeling off, the CZTS film was still strongly bound to the substrate, and the efficiency retained 91 % of the initial values (as shown in Figure S5), suggesting the good mechanical stability of the prepared CE.

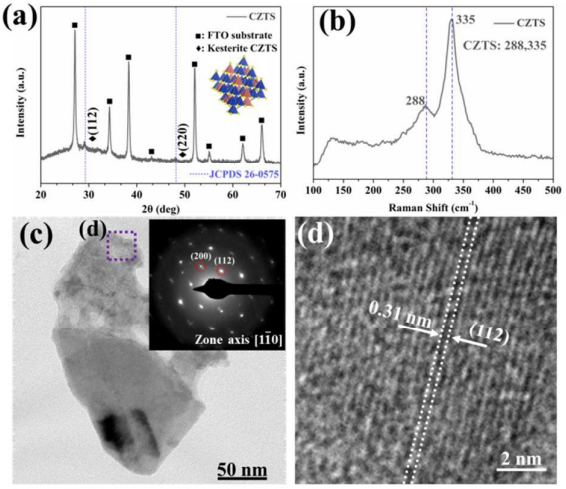

Figure 2. (a) XRD patterns and (b) Raman spectra of the as-synthesized CZTS CE on FTO substrate, exhibiting the well-defined signals assigned to kesterite-structure CZTS phase (JCPDS no. 26-0575). (c) TEM images of the rounded CZTS nanosheet. The insert shows the corresponding SAED pattern. (d) HR-TEM image of a single nanosheet scraped from the CZTS film. The insert shows the magnification picture of layered CZTS nanosheet.

The electrocatalytic activity of the CZTS and Pt electrode was evaluated by cyclic voltammetry (CV) measurements in triiodide electrolyte. Figure 3 (b) shows that rounded CZTS nanosheet CE has excellent electrochemical stability in I^-/I_3^- solutions. Two typical pairs of oxidation and reduction peaks appear in CV curves for both CE samples. The redox peaks at more negative potentials, represented by peak I and peak I′, correspond to the reduction of I_3^- to I^-, and the redox peaks at more positive potentials, represented by peak II and peak II′′, correspond to the oxidation of I^- to I_3^-:[17]

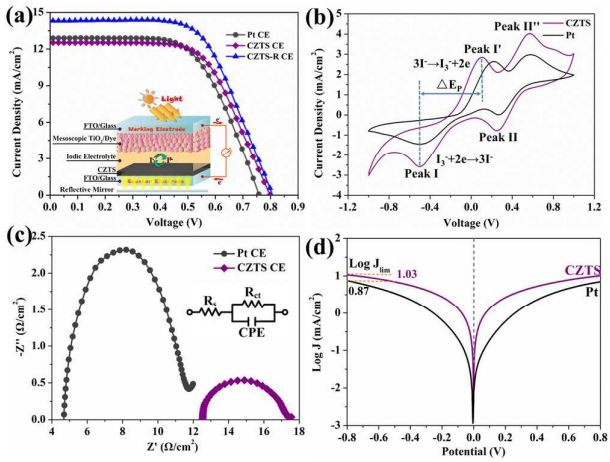

Figure 3. (a) J-V characteristics of DSSCs with Pt and CZTS films as CEs under a light intensity of 100 mW/cm^2 (1 sun). (b) Cyclic voltammograms of Pt and CZTS electrodes measured in an acetonitrile solution containing 1 mM I_2, 10 mM LiI, and 0.1 M $LiClO_4$ at a scan rate of 100 mV/s. (c) Nyquist plots for the I_3^-/I^- symmetrical cells based on Pt and CZTS CE under a bias of 0 V. (d) Tafel plots of Pt and CZTS symmetrical cells between ±0.8 V with a scan rate of 10 mV at room temperature.

Two main parameters from CV curve represent the overall electrocatalytic abilities towards the reduction of I_3^- to I^-; they are: (1) the peak-to-peak separation (ΔE_P) and (2) the cathodic peak current density (I_P) at more negative potential. The CZTS nanosheet CE demonstrates higher I_P values than that of the commercial Pt, for both the anodic and cathodic sides. It is implied that the electrocatalytic ability of the rounded CZTS nanosheet networks towards I^-/I_3^- redox couple is better than that of Pt CE, in accordance with the observations from previous literature.[32-34] In addition, the value of ΔE_P (0.60 V) for CZTS is small than that of the Pt (0.71 V), and the peak position of reduction reaction is nearly the same, confirming the higher catalytic activity toward the reduction of triiodide. Furthermore, the catalytic reaction is a kinetic process, which is related to the electron transfer rate constant and the number of active sites. The area of Peak I′ is wider for the rounded CZTS nanosheet networks than that for Pt, indicating that the CZTS nanostructure has provided more catalytic reaction sites than the Pt CE. The long-term stability of the CZTS CE was also tested against I^-/I_3^- electrolyte by subjecting the electrodes to 20 potential successive cycles, as shown in Figure S6. The value of I_P decreases by about 14 % after 20 cycles of potential scanning. Thus, the rounded CZTS nanosheet networks CE has superior catalytic activity properties compared to Pt. The conclusion from the CV data is consistent with previous PCE results. The electron conductivity, mass diffusion and catalytic activity of as-obtained CZTS could be effectively derived from electrochemical impedance spectroscopy (EIS), which was conducted on the symmetrical CZTS and Pt

electrochemical cells, as shown in Figure 3 (c). The detailed electrochemical parameters of the symmetrical cells extracted by fitting the EIS spectra are summarized in Table S2, including R_S, R_{Ct}, and C_μ value. The R_S value is mainly composed of the resistance of the FTO substrate, the bulk resistance of CZTS, and the contact resistance. The smaller bulk resistance of CZTS and the better adhesion between catalytic layer the substrate are responsible for the smaller R_S values. The R_S value of CZTS CEs (12.44 Ω/cm^2) is low, reflecting a good conductivity and bonding strength between in-situ CZTS film and FTO substrate, which in turn promotes the transfer of more electrons from the external circuit or of holes from the electrolyte to the CEs.[52] Furthermore, the R_S greatly affects the FF and J_{SC} of the solar cell, with higher FF and J_{SC} resulting from smaller R_S value, which is consistent with the result of photovoltaic performance. It is also worth noting that the in-situ grown nanostructure CZTS film exhibits R_{Ct} values (4.82 Ω/cm^2) that are well below the 10 Ω/cm^2 level needed for high-performance solar cells, and even smaller than that of the Pt electrode, suggesting the eximious catalytic activity of CZTS CE.[15] The small value of R_{Ct} is due to the high contact surface area and fast electron-transfer pathway of CZTS nanosheet networks. In addition, a high C_μ value (11.94 μF) represents a large surface area of the CZTS CE, concordant with the results obtained from the FE-SEM. Accordingly, the rounded CZTS nanosheet networks CE shows high active catalytic properties for the reduction of I_3^-, which agrees well with the CV results. To support EIS and CV data, Tafel polarization measurement was also carried out with the same symmetrical cells to further confirm the contribution of electron-transfer rate to the improvement of PCE. It can be seen in Figure 3 (d) that the CE with CZTS nanosheet shows the higher J_0 than Pt, suggesting the better electrocatalytic activity, in good agreement with the tendency of the cathodic peak current observed in CV profile. The J_0 value is directly related to the charge transfer resistance (R_{Ct}) and is supplied by the following eqn 4, thus reconfirming the smaller charge transfer resistance on the CZTS electrode.[52] The above observation is well consistent with the results for R_{Ct} values revealed by EIS spectra.

$$J_0=RT/nFR_{Ct} \qquad (4)$$

where R is the gas constant, T is the absolute temperature in K, n is the number of electrons involved in the electrochemical reduction reaction, F is the Faraday constant, and R_{Ct} is the charge transfer resistance at the CE/electrolyte interface obtained from EIS spectra. The limiting diffusion current density (J_{lim}) is also deduced from the Tafel curve at high potential. J_{lim} is closely related to the catalytic activity of the catalyst. The J_{lim} value of the CZTS electrode (1.03 mA/cm^2) is higher than that that of the Pt electrode (0.87 mA/cm^2), demonstrating a higher diffusion coefficient, as shown in eqn 5. J_{lim} depends on the diffusion coefficient of the redox couple in the electrolyte. This Tafel polarization result is consistent with the EIS and CV results.

$$D=lJ_{lim}/2nFC \qquad (5)$$

where D is the diffusion coefficient of the I_3^-, l is the electrolyte thickness, n is the number of electrons involved in the reduction of I_3^- at the counter electrode, F is the Faraday constant, and C is the iodic concentration.

Table 1. Photovoltaic parameters for DSSCs assembled with Pt and CZTS CE under 1 sun Illumination (AM 1.5G, 100 mW cm^{-2})

CE	J_{SC} (mA/cm^2)	V_{OC} (V)	FF (%)	η (%)
CZTS	12.52±0.45	0.79±0.01	62.92±0.09	6.24±0.15
CZTS-R	14.31±0.37	0.80±0.01	62.16±0.05	7.12±0.13
Pt	12.90±0.28	0.76±0.01	61.42±0.04	6.01±0.14

The semi-transparent rounded CZTS nanosheet networks were in-situ grown on FTO glass substrate, via a feasible solution method, based on room temperature electrodeposition and solvothermal treatment. The electrodeposited CZT precursor film was completely converted to CZTS nanosheet networks after a mild solvothermal treatment. The corresponding SAED pattern of the tetragonal-structure CZTS nanosheet demonstrated its single crystals with great crystallinity. The DSSCs assembled with rounded CZTS nanosheet networks show the power conversion efficiency (PCE) of 6.24 %, which was higher than that of Pt (6.01 %). It is noted that, PCE increased to 7.12 % under assisted by a mirror. The expanded catalytic surface area, high photo-generated electron injection at the counter electrode/redox electrolyte interface, great electrocatalytic activity for I_3^- reduction, low charge transfer resistance toward the reduction of I_3^- ions, and high diffusion coefficient of the I_3^- boost the improved performance of DSSCs. However, it is still noteworthy that, though relatively good long-term stability of CZTS CE in the electrolyte has been confirmed by conducting reproducibility measurement, peel-off test, and consecutive CV scans, the real long-term stability of these integrated solar cell devices and first-principle density functional theory (DFT) calculation are still needed to be further assessed and conducted, as this should be of great importance for their practical applications, and, we will continue to work on this issue.

The authors are grateful for the support from the National Nature Science Foundation of China (Grant no. 51202112), the Priority Academic Program Development of Jiangsu Higher Education Institutions (PAPD), the Foundation of Graduate Innovation Center in NUAA (Grant no. KFJJ201442), the Fundamental Research Funds for the Central Universities (Grant no. NJ20150027), and the Open Fund of Jiangsu Key Laboratory of Materials and Technology for Energy Conversion (Grant no. MTEC-2015M04).

Notes and references

1 K. Anderson, A. Bows and Philos. *Trans. R. Soc. A*, 2011, **369**, 20-44.
2 M.M. Lee, J. Teuscher, T. Miyasaka, T.N. Murakami and H.J. Snaith, *Science*, 2012, **338**, 643-647.

3 C.K. Chan, H.L. Peng, G. Liu, K. McIlwrath, X.F. Zhang, R.A. Huggins and Y. Cui, *Nat. Nanotechnol.*, 2008, **3**, 31-35.
4 B. O'Regan and M. Gratzel, *Nature*, 1991, **353**, 737-740.
5 P. Docampo, S. Guldin, T. Leijtens, N.K. Noel, U. Steiner and H.J. Snaith, *Adv. Mater.*, 2014, **26**, 4013-4030.
6 S. Mathew, A. Yella, P. Gao, R. Humphry-Baker, B.F.E. Curchod, N. Ashari-Astani, I. Tavernelli, U. Rothlisberger, K. Nazeeruddin Md and M. Grätzel, *Nat. Chem.*, 2014, **6**, 242-247.
7 M.I. Asghar, K. Miettunen, J. Halme, P. Vahermaa, M. Toivola, K. Aitola and P. Lund, *Energy Environ. Sci.*, 2010, **3**, 418-426.
8 S. Thomas, T.G. Deepak, G.S. Anjusree, T.A. Arun, S.V. Naira and A.S. Nair, *J. Mater. Chem. A*, 2014, **2**, 4474-4490.
9 M. Wu and T. Ma, *J. Phys. Chem. C*, 2014, **118**, 16727-16742.
10 J. Ma, C. Li, F. Yu and J. Chen, *ChemSusChem*, 2014, **7**, 3304-3311.
11 Y. Xiao, J. Wu, J. Lin, G. Yue, J. Lin, M. Huang, Y. Huang, Z. Lan and L. Fan, *J. Mater. Chem. A*, 2013, **1**, 13885-13889.
12 G. Liu, H. Wang, X. Li, Y. Rong, Z. Ku, M. Xu, L. Liu, M. Hu, Y. Yang, P. Xiang, T. Shu and H. Han, *Electrochim. Acta*, 2012, **69**, 334-339.
13 G. Veerappan, K. Bojan and S.W Rhee, *ACS Appl. Mater. Inter.*, 2011, **3**, 857-862.
14 Y.F. Lin, C.T. Li and K.C. Ho, *J. Mater. Chem. A*, 2015, DOI: 10.1039/C5TA06376K.
15 F. Liu, J. Zhu, Y. Xu, L. Zhou, Y. Li, L. Hu, J. Yao and S. Dai, *Chem. Commun.*, 2015, **51**, 8108-8111.
16 F. Liu, J. Zhu, L. Hu, B. Zhang, J. Yao, M.K. Nazeeruddin, M. Grätzel and S. Dai, *J. Mater. Chem. A*, 2015, **3**, 6315-6323.
17 W. J. Wang, X. Pan, W. Q. Liu, B. Zhang, H. W. Chen, X. Q. Fang, J. X. Yao and S. Dai, *Chem. Commun.*, 2014, **50**, 2618-2620.
18 F. Gong, H. Wang, X. Xu, G. Zhou and Z. S. Wang, *J. Am. Chem. Soc.*, 2012, **134**, 10953-10958.
19 H.W. Chen, C.W. Kung, C.M. Tseng, T.C. Wei, N. Sakai, S. Morita, M. Ikegami, T. Miyasaka and K.C. Ho, *J. Mater. Chem. A*, 2013, **1**, 13759-13768.
20 F. Gong, X. Xu, Z. Li, G. Zhou and Z. S. Wang, *Chem. Commun.*, 2013, **49**, 1437-1439.
21 X. Sun, J. Dou, F. Xie, Y. Li and M. Wei, *Chem. Commun.*, 2014, **50**, 9869-9871.
22 W. Ke, G. Fang, H. Tao, P. Qin, J. Wang, H. Lei, Q. Liu and X. Zhao, *ACS Appl. Mater. Interfaces*, 2014, **6**, 5525-5530.
23 Z. Li, F. Gong, G. Zhou and Z.S. Wang, *J. Phys. Chem. C*, 2013, **117**, 6561-6566.
24 J. Zheng, W. Zhou, Y. Ma, W. Cao, C. Wang and L. Guo, *Chem. Commun.*, 2015, **51**, 12863-12866.
25 Z. Wan, C. Jia and Y. Wang, *Nanoscale*, 2015, **7**, 12737-12742.
26 H. Zhang, M. Ge, L. Yang, Z. Zhou, W. Chen, Q. Li and L. Liu, *J. Phys. Chem. C*, 2013, **117**, 10285-10290.
27 S. Jiang, X. Yin, J. Zhang, X. Zhu, J. Li and M. He, *Nanoscale*, 2015, **7**, 10459-10464.
28 H. Chen, Y. Xie, H. Cui, W Zhao, X. Zhu, Y. Wang, X. Lu and F. Huang, *Chem. Commun.*, 2014, **50**, 4475-4477.
29 J. Yang, C. Bao, J. Zhang, T. Yu, H. Huang, Y. Wei, H. Gao, G. Fu, J. Liu and Z. Zou, *Chem. Commun.*, 2013, **49**, 2028-2030.
30 R.R. Prabhakar, N.H. Loc, M.H. Kumar, P.P. Boix, S. Juan, R.A. John, S.K. Batabyal and L.H. Wong, *ACS Appl. Mater. Interfaces*, 2014, **6**, 17661-17667.
31 X. Xin, M. He, W. Han, J. Jung and Z. Lin, *Angew. Chem., Int. Ed.*, 2011, **50**, 11739-11742.
32 Y.F. Du, J.Q. Fan, W.H. Zhou, Z.J. Zhou, J. Jiao and S.X. Wu, *ACS Appl. Mater. Interfaces*, 2012, **4**, 1796-1802.
33 S. Wozny, K. Wang and W. Zhou, *J. Mater. Chem. A*, 2013, **1**, 15517-15523.
34 M.S. Fan, J.H. Chen, C.T. Li, K.W. Cheng and K.C. Ho, *J. Mater. Chem. A*, 2015, **3**, 562-569.
35 S.S. Mali, P.S. Patil and C.K. Hong, *ACS Appl. Mater. Interfaces*, 2014, **6**, 1688-1696.
36 S.K. Swami, N. Chaturvedi, A. Kumar, N. Chander, V. Dutta, D.K. Kumar, A. Ivaturi, S. Senthilarasu and H.M. Upadhyaya, *Phys. Chem. Chem. Phys.*, 2014, **16**, 23993-23999.
37 X. Zeng, D. Xiong, W. Zhang L. Ming, Z. Xu, Z. Huang, M. Wang, W. Chen and Y.B. Cheng, *Nanoscale*, 2013, **5**, 6992-6998.
38 Y. Zhang, C. Shi, X. Daia, F. Liu, X. Fang and J. Zhu, *Electrochim. Acta*, 2014, **118**, 41-44.
39 K. Cheng, J. Meng, X. Wang, Y. Huang, J. Liu, M. Xue and Z. Du, *Mater. Chem. Phys.*, 2015, **163**, 24-29.
40 Y. Xie, C. Zhang, F. Yue, Y. Zhang, Y. Shi and T. Ma, *RSC Adv.*, 2013, **3**, 23264-23268.
41 P. Dai, G. Zhang, Y. Chen, H. Jiang, Z. Feng, Z. Lin and J. Zhan, *Chem. Commun.*, 2012, **48**, 3006-3008.
42 J. Xu, X. Yang, Q.D. Yang, T.L. Wong and C.S. Lee, *J. Phys. Chem. C*, 2012, **116**, 19718-19723.
43 J. Liu, F. Luo, A. Wei, Z. Lia and Y. Zhao, *Mater. Lett.*, 2015, **141**, 228-230.
44 N. Fu, X. Xiao, X. Zhou, J. Zhang and Y. Lin, *J. Phys. Chem. C*, 2012, **116**, 2850-2857.
45 R. Akbarzadeh, H. Dehghani and F. Behnoudnia, *Dalton Trans.*, 2014, **43**, 16745-16753.
46 R. Akbarzadeh and H. Dehghani, *Dalton Trans.*, 2014, **43**, 5474-5481.
47 C.W. Kung, H.W. Chen, C.Y. Lin, K.C. Huang, R. Vittal and K.C. Ho, *ACS Nano*, 2012, **6**, 7016-7025.
48 J. Ma, C. Li, F. Yu and J. Chen, *ChemSusChem*, 2014, **7**, 3304-3311.
49 W. Guo, X. Zhang, R. Yu, M. Que, Z. Zhang, Z. Wang, Q. Hua, C. Wang, Z.L. Wang and C. Pan, *Adv. Energy Mater.*, 2015, **5**, 1500141.
50 E. Vayner, R.A. Sidik and A.B. Anderson, *J. Phys. Chem. C*, 2007, **111**, 10508-10513.
51 S. Das, P. Sudhagar, S. Nagarajan, E. Ito, S.Y. Lee, Y.S. Kang and W. Choi, *Carbon*, 2012, **50**, 4815-4821.
52 C.V.V.M. Gopi, S.S. Rao, S.K. Kim, D. Punnoose and H.J. Kim, *J. Power Sources*, 2015, **275**, 547-556.

Rounded Cu2ZnSnS4 Nanosheet Networks as Cost-effective Counter Electrode for High-Efficiency Dye-Sensitized Solar Cells

Shan-Long Chen,[ab] Jie Tao,[a*] Hai-Jun Tao,[ab] Yi-Zhou Shen,[a] Ai-Chun Xu,[a] Fang-Xu Cao,[a] Jia-Jia Jiang,[a] Tao Wang[a] and Lei Pan[a]

Graphical Abstract